

Impact of Anthropogenic CO₂ on the CaCO₃ System in the Oceans

Richard A. Feely,^{1,*} Christopher L. Sabine,¹ Kitack Lee,²
Will Berelson,³ Joanie Kleypas,⁴ Victoria J. Fabry,⁵
Frank J. Millero⁶

Rising atmospheric carbon dioxide (CO₂) concentrations over the past two centuries have led to greater CO₂ uptake by the oceans. This acidification process has changed the saturation state of the oceans with respect to calcium carbonate (CaCO₃) particles. Here we estimate the in situ CaCO₃ dissolution rates for the global oceans from total alkalinity and chlorofluorocarbon data, and we also discuss the future impacts of anthropogenic CO₂ on CaCO₃ shell-forming species. CaCO₃ dissolution rates, ranging from 0.003 to 1.2 micromoles per kilogram per year, are observed beginning near the aragonite saturation horizon. The total water column CaCO₃ dissolution rate for the global oceans is approximately 0.5 ± 0.2 petagrams of CaCO₃-C per year, which is approximately 45 to 65% of the export production of CaCO₃.

Atmospheric CO₂ concentrations oscillated between 200 and 280 parts per million (ppm) over the 400,000 years before the industrial period. Current atmospheric concentrations are now approaching 380 ppm as a result of the industrial and land use activities of humankind. In the past few decades, only half of the CO₂ released by human activity has remained in the atmosphere; of the remainder, about 30% has been taken up by the ocean and 20% by the terrestrial biosphere (1).

Most previous estimates of oceanic uptake of CO₂ were made using ocean circulation models calibrated with tracer observations. Recently, a large global data set of ocean tracer and carbon system observations has been acquired through the World Ocean Cir-

culatation Experiment/Joint Global Ocean Flux Study. These observations indicate a total ocean uptake of anthropogenic CO₂ of approximately 118 ± 19 Pg of C (1 Pg of C = 10¹⁵ g of C) between 1800 and 1994 (1).

Estimates of future atmospheric and oceanic CO₂ concentrations, based on the Intergovernmental Panel on Climate Change emission scenarios and general circulation models, suggest that by the end of the century CO₂ levels could be over 800 ppm (2). Corresponding models for the oceans indicate that surface-water dissolved inorganic carbon (DIC) could probably increase by more than 12%, and the carbonate ion concentration would decrease by almost 60% (3) (Fig. 1). The corresponding pH drop would be

about 0.4 pH units in surface waters (4). Such dramatic changes of the CO₂ system in open-ocean surface waters have probably not occurred for more than 20 million years of Earth's history. If they do occur, they can potentially have significant impacts on the biological systems in the oceans in ways we are only beginning to understand (5). Thus, the delicate balance of marine planktonic species could undergo significant shifts in the future as humankind continues along the path of unintentional CO₂ sequestration in the surface oceans.

Concern about the long-term fate of anthropogenic CO₂ in the atmosphere and ocean has motivated scientists to examine the distributions of DIC and total alkalinity (TA) in the oceans. Processes that increase the TA in the upper ocean facilitate the uptake of anthropogenic CO₂ from the atmosphere. The dissolution of marine carbonates, including biogenic magnesian calcites (from coralline algae), aragonite (from corals and pteropods),

¹Pacific Marine Environmental Laboratory, National Oceanic and Atmospheric Administration, Seattle, WA 98115-6349, USA. ²School of Environmental Science and Engineering, Pohang University of Science and Technology, San 31, Nam-gu, Hyoja-dong, Pohang, 790-784, Republic of Korea. ³Department of Earth Sciences, University of Southern California, Los Angeles, Los Angeles, CA 90089-0740, USA. ⁴Environmental and Societal Impacts Group, National Center for Atmospheric Research, Boulder, CO 80307-3000, USA. ⁵Department of Biological Sciences, California State University San Marcos, San Marcos, CA 92096-0001, USA. ⁶University of Miami/Rosenstiel School of Marine and Atmospheric Sciences, Miami, FL, USA.

*To whom correspondence should be addressed. E-mail: richard.a.feely@noaa.gov

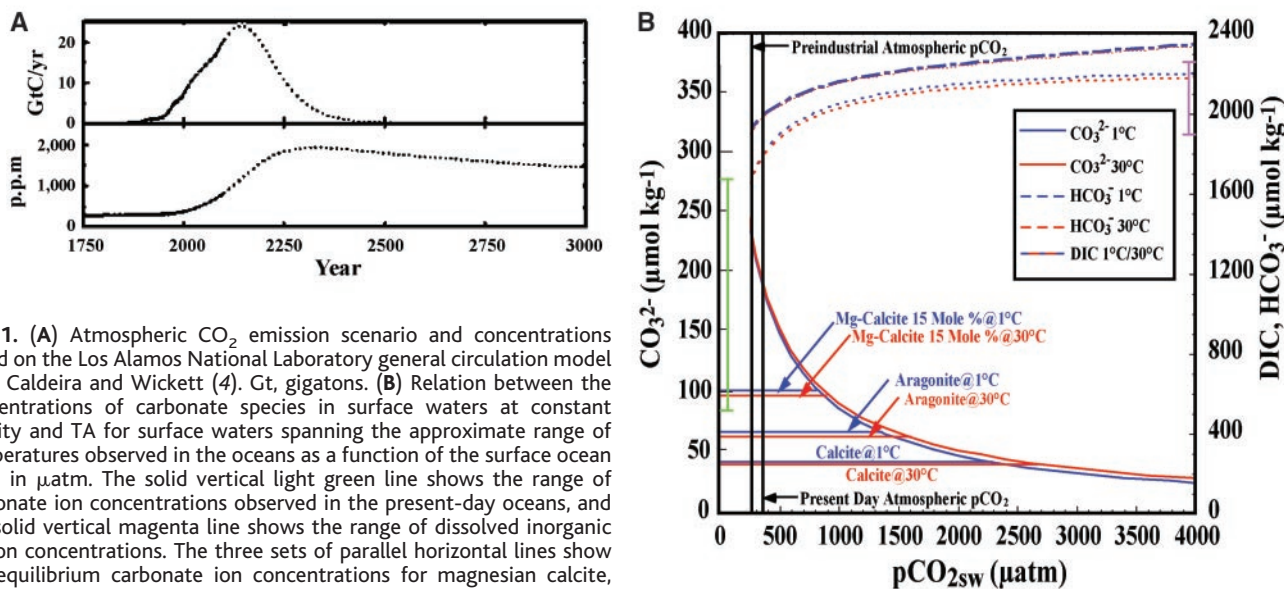


Fig. 1. (A) Atmospheric CO₂ emission scenario and concentrations based on the Los Alamos National Laboratory general circulation model after Caldeira and Wickett (4). Gt, gigatons. (B) Relation between the concentrations of carbonate species in surface waters at constant salinity and TA for surface waters spanning the approximate range of temperatures observed in the oceans as a function of the surface ocean pCO₂ in µatm. The solid vertical light green line shows the range of carbonate ion concentrations observed in the present-day oceans, and the solid vertical magenta line shows the range of dissolved inorganic carbon concentrations. The three sets of parallel horizontal lines show the equilibrium carbonate ion concentrations for magnesian calcite, aragonite, and calcite saturation, respectively.

and calcite (from coccolithophorids and foraminifera) neutralizes anthropogenic CO_2 and adds to TA via the reaction



The primary contributors to this reaction are the carbonate shells of marine plankton that are produced in the euphotic zone. Upon death, these carbonate tests fall through the water column and are either dissolved or deposited in shallow or deep-sea sediments. As the oceans become enriched in anthropogenic CO_2 , the locations and extent of dissolution will increase as a function of the decrease in the calcium carbonate (CaCO_3) saturation state. Until recently, it had been commonly thought that the dissolution of pelagic CaCO_3 particles primarily occurs at great depths below the calcite saturation depth (6). However, recent analyses of the global carbonate budget and carbonate data for the global oceans (7–9) have indicated that perhaps as much as 60 to 80% of the CaCO_3 that is exported out of the surface ocean dissolves in the upper 1000 m.

Calcite and aragonite saturation in the global oceans. The degree of saturation of seawater with respect to aragonite and calcite (Ω_{arg} or Ω_{cal}) is the ion product of the concentrations of calcium and carbonate ions, at the in situ temperature, salinity, and pres-

sure, divided by the stoichiometric solubility product (K_{sp}^*) for those conditions

$$\Omega_{\text{arg}} = [\text{Ca}^{2+}][\text{CO}_3^{2-}] / K_{\text{sparg}}^* \quad (2)$$

$$\Omega_{\text{cal}} = [\text{Ca}^{2+}][\text{CO}_3^{2-}] / K_{\text{spcal}}^* \quad (3)$$

where the calcium concentration is estimated from the salinity, and the carbonate ion concentration is calculated from the DIC and TA data. Because the calcium- to-salinity ratio in seawater does not vary by more than 1.5%, variations in the ratio of $[\text{CO}_3^{2-}]$ to the stoichiometric solubility product primarily govern the degree of saturation of seawater with respect to aragonite and calcite (Fig. 2). There is pronounced shoaling of both the aragonite and calcite saturation horizons from the Atlantic through the Indian to the Pacific Oceans because of the higher DIC/TA ratios in the intermediate and deep waters of the Indian and Pacific relative to the Atlantic. This is due to the cumulative enrichment of DIC relative to TA resulting from respiration processes as ocean water circulates along the deep conveyor belt from the Atlantic to Indian and Pacific (10, 11). The intermediate waters of the North Pacific show evidence for undersaturation in the shallow waters from 200 to 1000 m, where they have also been affected by anthropogenic CO_2 (12). Surprisingly, portions of the northern Indian Ocean

and southeastern Atlantic Ocean are also undersaturated with respect to aragonite at shallow depths, and this region also appears to be increasing in areal extent as a consequence of anthropogenic CO_2 accumulations (13–15). This can best be shown by plotting vertical sections of the present-day (solid line) and preindustrial (dashed line) saturation horizons superimposed on the anthropogenic CO_2 contours from data collected along the axis of the three basins (Fig. 3). The preindustrial levels are calculated by subtracting the anthropogenic CO_2 values from the total DIC. A comparison of the preindustrial and present-day saturation horizons reveals several distinct regions where the undersaturation zone has expanded. In regions between 20°N and 50°N in the North Atlantic Ocean, the aragonite saturation horizon for the preindustrial era is nearly the same as today (Fig. 3). In the eastern South and North Atlantic, however, the aragonite saturation horizon has migrated upward by approximately 80 to 150 m between 50°S and 15°N. In the Indian Ocean, saturation depths have shoaled increasingly north of 30°S, so that aragonite saturation depths in the Arabian Sea and Bay of Bengal are now 100 to 200 m shallower than in preindustrial times. In the Pacific, the upward migration of the aragonite saturation horizon is between 30 and 80 m south of 38°S and between 30 and 100 m north of 3°N. The calcite saturation horizon has also shoaled by about 40 to 100 m north of 20°N in the North Pacific. Such shoaling is due to the effects of anthropogenic CO_2 ventilation and biological respiration processes in the intermediate waters. This also implies that the dissolution of CaCO_3 particles will likely increase as the waters become increasingly undersaturated over time.

CaCO_3 dissolution. The amount of CaCO_3 dissolved in a subsurface water parcel (ΔCaCO_3) is estimated from changes in TA by subtracting out the preformed TA concentration and correcting for the TA decrease resulting from the release of protons during the oxidation of organic matter (12, 13) according to the equation

$$\begin{aligned} \Delta\text{CaCO}_3 (\mu\text{mol kg}^{-1}) = & \\ & 0.5 \times (\text{TA}_{\text{MEAS}} - \text{TA}^\circ) + \\ & 0.63(0.0941 \times \text{AOU}) \quad (4) \end{aligned}$$

where TA_{MEAS} is the measured TA, TA° is the preformed TA, and AOU is apparent oxygen utilization. The second term on the right-hand side accounts for the decrease in TA resulting from the oxidation of organic matter by using AOU [O_2 (saturated values at a given temperature and salinity) – O_2 (measured)] and the N/ O_2 ratio (= 0.094 ± 0.02) (16). A coefficient of 0.63 proposed by Kanamori and Ikegami (17) is used to account for TA contributions from the oxidation of organic nitrogen, phosphorus, and sulfur. The

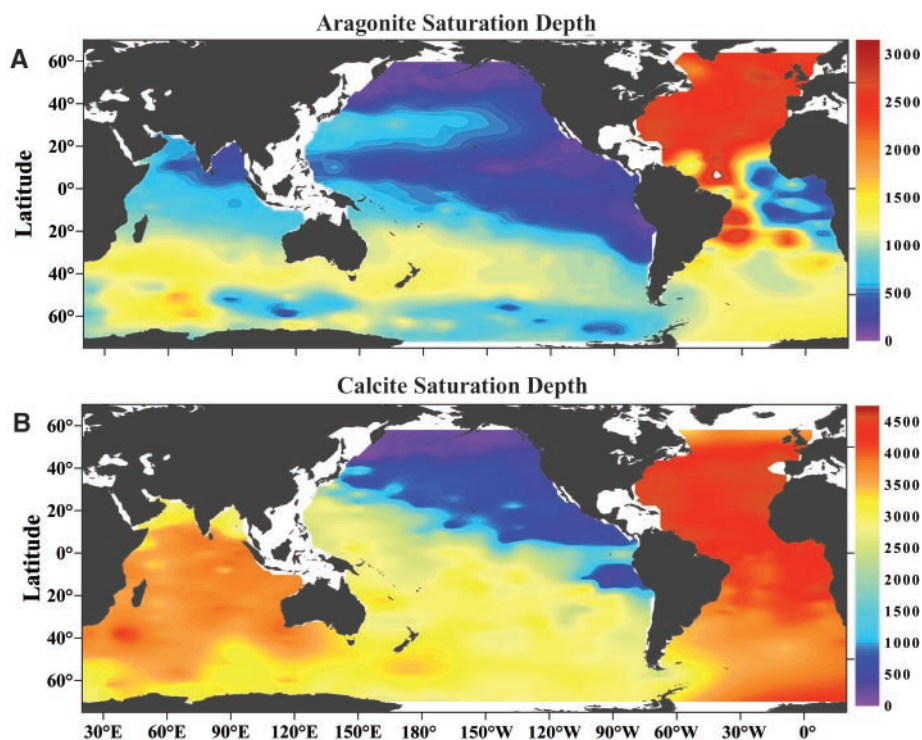


Fig. 2. Distribution of (A) aragonite and (B) calcite saturation depth ($\Omega = 1$) in the global oceans. The pressure effect on the solubility is estimated from the equation of Mucci (31) that includes the adjustments to the constants recommended by Millero (45). The level at which aragonite and calcite are in thermodynamic equilibrium is known as the saturation depth. When the degree of saturation, Ω , is greater than 1, seawater is supersaturated with aragonite and calcite; conversely, seawater is undersaturated with respect to these minerals when $\Omega < 1$. This depth is significantly shallower for aragonite than for calcite, because aragonite is more soluble in seawater than calcite.

TA° is estimated for each ocean basin with a multiparameter linear regression model using conservative tracers, such as salinity and NO or PO, as independent variables. NO is defined as $NO = O_2 - R_{O_2N} \times N$ (16); we used $R_{O_2N} = -10.625$ (16). The standard error (1σ) of the estimated TA° is $\sim 10 \mu\text{mol kg}^{-1}$.

To estimate in situ CaCO_3 dissolution rates in waters where values of ΔCaCO_3 are positive, we plotted ΔCaCO_3 against water parcel ages derived from chlorofluorocarbon-11 (CFC-11) or CFC-12 for the upper ocean and from ^{14}C for deep waters where CFC-11 or CFC-12 is not detected (18). The highest CaCO_3 dissolution rates in the North Atlantic occur near or below the average aragonite saturation horizon at approximately 3500 m (Fig. 4). The change in depth where the maximum rate occurs is consistent with the corresponding changes in the aragonite 100% saturation horizon. In the South Atlantic, CaCO_3 dissolution rates reach a maximum ($\sim 0.55 \mu\text{mol kg}^{-1} \text{ year}^{-1}$) near 900 m, decreasing to less than half that below 1250 m.

In the Indian Ocean, the highest CaCO_3 dissolution rates occur in shallow waters south of 20°S, with rates ranging from 0 to $1.2 \mu\text{mol kg}^{-1} \text{ year}^{-1}$ occurring between 200 and 1400 m. North of 20°S, the CaCO_3 dissolution maximum corresponds to a depth of about 250 m. In the Pacific, the highest dissolution rates (up to $\sim 1.2 \mu\text{mol kg}^{-1} \text{ year}^{-1}$) occur between 400 and 600 m, within the core of the North Pacific Intermediate Water. Significantly lower rates are observed below these depths. The large spatial differences in the patterns of the dissolution rates between the three major ocean basins appear to be related to the positions of the aragonite and calcite saturation horizons. The integrated carbonate dissolution rate for the three major ocean basins is estimated to be $0.5 \pm 0.2 \text{ Pg of CaCO}_3\text{-C year}^{-1}$, or about 45 to 65% of the export flux of CaCO_3 in the global oceans.

Sediment trap fluxes. Sediment traps measure the rain of particulate matter through the water column. Traps located at different depths at the same location can be used to

estimate the dissolution rate of CaCO_3 particles between those two depths. This approach has well-recognized caveats: It assumes that particles fall vertically between one trap and another, that both traps collect particles with equal efficiency, and that particles are not altered inside the trap collection cup. Traps deployed between 100 and 1000 m indicate dissolution rates (Table 1; 0.02 to $0.67 \mu\text{mol kg}^{-1} \text{ year}^{-1}$) that are comparable to the rates presented here. However, sediment traps at any depth, particularly those moored <1000 m below the ocean surface, can have high CaCO_3 flux losses and may be suspect because of over- and undertrapping artifacts caused by current turbulence or by the addition of heterotrophs swimming into the trap. Thus, there is a lower degree of confidence in this approach when shallow data are included. The deepwater sediment trap data, also presented in Table 1, are from sites in the equatorial and North Pacific Ocean and represent deployments of paired traps that collected particles for at least 200 days. Generally, traps in deeper water are considered more reliable in collecting vertical particle fluxes. In 9 of 10 data sets, there is evidence of carbonate dissolution occurring in the water column between 1000 and 4500 m in the Pacific Ocean. Dissolution rates in the deep water are low, ranging from 0.003 to $0.03 \mu\text{mol kg}^{-1} \text{ year}^{-1}$. These values are consistent with the estimates of carbonate dissolution in the deep Pacific (12) insofar as they do not exceed the water-mass tracer results; the water-mass tracer method allows for dissolution both in the water column and in surface sediments, whereas the trap data measures dissolution in the water column only. The very low particle dissolution rates in the deep-water column of the tropical and subtropical regions imply a greater role for sedimentary dissolution in these areas. In the northeastern subarctic Pacific, however, carbonate particle dissolution in the water column may contribute 20 to 80% of the total dissolution burden predicted by the water-mass approach. The highest rate determined by this trap summary is for a site in the northeastern North Pacific, which suggests that water column dissolution may be more important than sediment dissolution at higher latitudes.

CaCO_3 budget of the global oceans.

The major components of the CaCO_3 budget have recently been reassessed (1, 9, 19) and are summarized in Fig. 5. Global new production of CaCO_3 ranges from 0.8 to 1.4 Pg of $\text{CaCO}_3\text{-C year}^{-1}$ (19, 20), based on models or observations of seasonal changes in alkalinity in the euphotic zone. The most recent updates of globally averaged sediment trap data through 2000 m indicate a global average flux of about 0.4 Pg of $\text{CaCO}_3\text{-C year}^{-1}$, suggesting that anywhere from 50 to 71% of the CaCO_3 produced is dissolved in the upper water column (19). This is consistent with our estimates of the water column dissolution of CaCO_3 , which show an average dissolu-

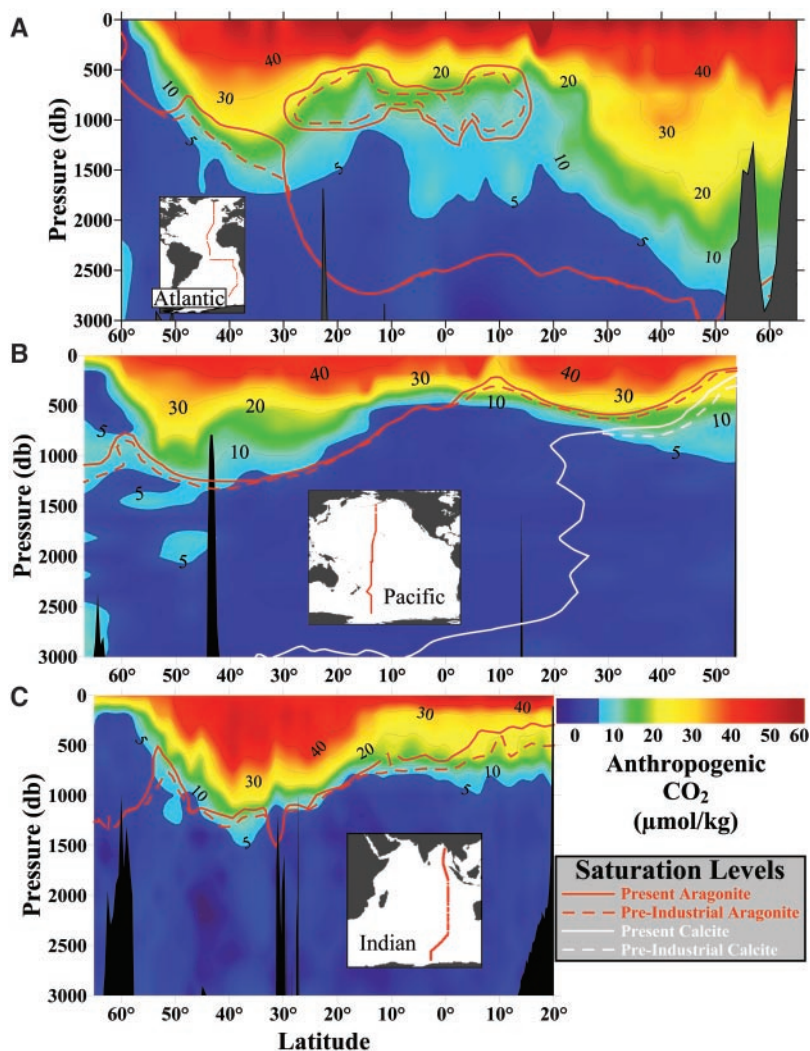


Fig. 3. Vertical distributions of anthropogenic CO_2 concentrations in $\mu\text{mol kg}^{-1}$ and the supersaturation/undersaturation horizons for aragonite and calcite along north-south transects in the (A) Atlantic, (B) Pacific, and (C) Indian Oceans.

tion of approximately 0.5 Pg of $\text{CaCO}_3\text{-C}$ year⁻¹ globally. It is also consistent with the recent summary of the fluxes of foraminiferal CaCO_3 tests in the oceans, which indicates that approximately 65% of the tests are dissolved in the upper 1000 m of the water column (21). The present-day accumulation of CaCO_3 in marine sediments is about 0.1 to 0.14 Pg of $\text{CaCO}_3\text{-C}$ year⁻¹ along the continental margins or in the deep sea, and 0.13 to 0.17 Pg of $\text{CaCO}_3\text{-C}$ year⁻¹ in continental shelf sediments (9, 19, 22). Thus, of the total amount of CaCO_3 that is produced annually, no more than about 30% is buried in shallow and deep sediments. The rest is dissolved in the water column, at the sediment-seawater interface or in the upper portion of the sediment column. These new results, however, indicate that a very large fraction of this dissolution, up to 60% or more, occurs in the upper water column above 2000 m.

Future impacts. The long-term impacts of anthropogenic CO_2 on the saturation state of the oceans with respect to aragonite and calcite particles in the oceans have been discussed previously (23, 24). In the cold high-latitude surface waters typical of the subarctic North Pacific, aragonite and calcite undersaturation will occur when partial pressure of CO_2 ($p\text{CO}_2$) values reach 1200 and 1900 μatm , respectively, and in warm tropical and subtropical waters when $p\text{CO}_2$ values reach 1700 and 2800 μatm , respectively (Fig. 1). These values are greater than what is normally observed in present-day surface waters (25), but if present trends in anthropogenic CO_2 continue for the next several hundred years, we can expect regions of aragonite undersaturation to develop in the northern subarctic surface waters, followed by calcite undersaturation. This would first occur in the winter, when $p\text{CO}_2$ values are highest because of cold temperatures and wind-driven mixing of subsurface waters into the mixed layer. From there, the progression of undersaturated regions would proceed toward the equator, although it is unlikely that the tropical and warmest subtropical surface waters will ever become undersaturated with respect to calcite, because model projections of CO_2 emissions predict an upper limit of atmospheric CO_2 of about 2000 μatm (4). Nevertheless, large-scale decreases in the aragonite and calcite saturation values over the global oceans can have profound impacts on calcification rates for many species of CaCO_3 shell-forming organisms.

Biological implications. Because the upper ocean is supersaturated with respect to all phases of CaCO_3 , carbonate chemistry was not previously considered as a limiting factor in biogenic calcification. Recent field and laboratory studies (table S1), however, reveal that the degree of supersaturation has a profound effect on the calcification rates of individual species and communities in both planktonic and benthic habitats. With one

exception (26), the calcification rate of all calcifying organisms investigated to date decreased in response to a decreased CaCO_3 saturation state, even when the carbonate saturation level was >1 . This response holds across multiple taxa—from single-celled protists to reef-building corals—and across all CaCO_3 mineral phases. Differences in the response of calcifiers to decreasing carbonate ion concentrations may reflect differences in carbonate mineralogy; in environmental parameters such as temperature, light, and available nutrients (27, 28); and in the mechanism of biomineralization (29, 30).

Aragonite and magnesian calcite are at least 50% more soluble in seawater than calcite (31), suggesting that organisms that form these types of CaCO_3 may be particularly affected by increasing $p\text{CO}_2$. Coralline algae, a major source of biogenic magnesian calcite, show a strong calcification response to de-

creases in saturation state. The main aragonite producers are reef-building corals and planktonic pteropod and heteropod molluscs. Nearly all reef-building corals tested so far show a marked decline in calcification under reduced $[\text{CO}_3^{2-}]$ conditions (27, 32, 33), and one of us (V.F.) has observed shell dissolution in living *Clio pyramidata*, a pteropod in the subarctic North Pacific, as increasing respiratory CO_2 forced aragonite saturation to <1 (fig. S1). The effects of elevated CO_2 on other producers of aragonite and magnesian calcite, including calcareous green algae, echinoderms, bryozoans, and benthic foraminifera, are unknown. Although these labile carbonate producers are associated with benthic habitats, in the North Atlantic many of them are also found in the open ocean encrusting on *Sargassum* clumps (34–36).

Calcite is secreted by two important planktonic calcifiers—coccolithophores and fora-

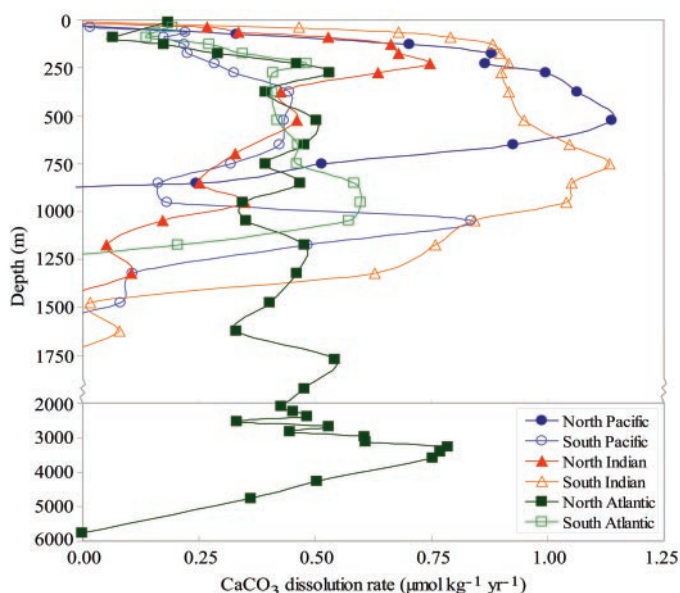


Fig. 4. In situ CaCO_3 dissolution rates plotted as a function of depth in the three major ocean basins.

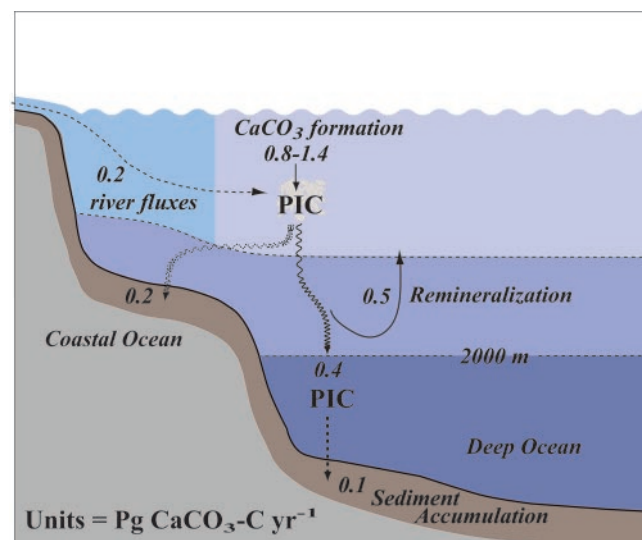


Fig. 5. Schematic diagram of the CaCO_3 budget for the global oceans. The values are in Pg of $\text{CaCO}_3\text{-C}$ year⁻¹.

Table 1. Sediment trap particulate CaCO₃ dissolution fluxes in the Pacific Ocean. The difference between the mean carbonate flux in the upper trap and the lower trap defines the dissolution flux. In all but one of the deepwater cases, the CaCO₃ flux collected in the midwater trap is higher than the carbonate flux collected in the deepwater trap. The dissolution rates are derived from the differences in CaCO₃ sediment trap fluxes between the upper and lower sediment traps divided by the depth range between the traps.

Location	Trap depth range (m)	Dissolution rate (μmol kg ⁻¹ year ⁻¹)	Reference
<i>Shallow sediment traps</i>			
Northwestern Pacific	100–1000	0.12	(46)
Equatorial Pacific	105–320	0.67	(47)
Northwestern Pacific	500–1000	0.02	(48)
Northeastern Pacific	200–1000	0.10	(49)
<i>Deep sediment traps</i>			
Northwestern Pacific	2000–4000	0.003–0.006	(48)
Equatorial Pacific	2300–3600	0.005–0.014	(50)
2°59.8'N 135°1.0'E	1592–3902	0.012	(51)
4°7.5'N 136°16.6'E	1769–4574	0.013	(51)
0°0.2'N 175°09.7'E	1357–4363	0.005	(51)
0°01'N 175°02'E	2200–4300	—	(52)
13°00'N 175°01'E	1500–5100	0.006	(52)
00°04'N 139°45'W	2284–3618	0.005–0.014	(50)
11°58'S 135°02'W	1292–3594	0.003	(52)
50°0'N 145°0'W	1000–3800	0.024	(49)

miniferans—and species in both groups appear to be sensitive to changes in seawater carbonate chemistry. The calcification rates of two bloom-forming coccolithophores, *Emiliania huxleyi* and *Gephyrocapsa oceanica*, decreased by 25 and 45%, respectively, when grown at *p*CO₂ concentrations that were three times the preindustrial values (37, 38). Shell weights of similarly sized planktonic foraminiferans have also been shown to vary because of the effects of seawater carbonate chemistry on both biological calcification and dissolution (39, 40). The available empirical evidence suggests that the relation between calcification and carbonate ion concentration in these coccolithophore and foraminiferan species is asymptotic, implying that reduction of the carbonate saturation state below a threshold value will lead to large decreases in calcification rates, even when saturation is >1.

At the global scale, calcium carbonate plays a dual role in regulating carbon sequestration by the oceans. First, an increase in CaCO₃ dissolution in the upper ocean will result in a more uniform alkalinity profile with depth. Presently, the TA of temperate surface waters is about 50 to 150 μmol kg⁻¹ less than in the deep oceans because carbonate precipitation in the upper ocean removes alkalinity, whereas dissolution of calcium carbonate at depth increases alkalinity. Moreover, a decrease in carbonate precipitation in the upper ocean would increase the capacity of the oceans to take up CO₂ from the atmosphere. A complete shutdown of surface ocean calcification would decrease surface ocean *p*CO₂ by about 10 to 20 μatm (41). Second, a decrease in CaCO₃ production would affect the ratio of organic:inorganic carbon delivery to the deep sea. If the processes regulating the “rain” of organic carbon and inorganic carbon to deep-sea sediments are uncoupled, then a decrease in calcium carbonate production

would lead to increased dissolution of calcium carbonate sediments, which would raise ocean pH and its capacity to store CO₂ (42). If the two processes are coupled, such as through the process of CaCO₃ ballasting of organic carbon (43), then reducing the carbonate production could result in shallower remineralization of organic carbon (44) and a diminished role of sediments in buffering increases in atmospheric CO₂. Clearly, more research on the mechanistic controls of these seemingly coupled processes is needed.

References and Notes

- C. L. Sabine et al., in *The Global Carbon Cycle: Integrating Humans, Climate, and The Natural World*. SCOPE 62, C. B. Field, M. R. Raupach Eds. (Island Press, Washington, DC, 2004), pp. 17–46.
- C. Prentice et al., in *Climate Change 2001: The Scientific Basis, Contribution of Working Group I to the Third Assessment Report of the Intergovernmental Panel on Climate Change*, J. Houghton et al., Eds. (Cambridge Univ. Press, New York, 2001), pp. 183–238.
- P. G. Brewer, *Geophys. Res. Lett.* **24**, 1367 (1997).
- K. Caldeira, M. E. Wickett, *Nature* **425**, 365 (2003).
- B. A. Seibel, V. J. Fabry, in *Climate Change and Biodiversity: Synergistic Impacts*, L. Hannah, T. Lovejoy, Eds. (Conservation International, Washington, DC, 2003), pp. 59–67.
- W. S. Broecker, in *The Fate of Fossil CO₂ in the Oceans*, N. R. Anderson, A. Malahoff, Eds. (Plenum, New York, 1977), pp. 207–212.
- J. D. Milliman, *Global Biogeochem. Cycles* **7**, 927 (1993).
- J. D. Milliman, A. W. Droxler, *Geol. Rundsch.* **85**, 496 (1996).
- J. D. Milliman et al., *Deep-Sea Res. Part I* **46**, 1653 (1999).
- W. S. Broecker, T.-H. Peng, *Tracers in the Sea* (Lamont-Doherty Geological Observatory, Palisades, New York, 1982).
- W. S. Broecker, in *Treatise on Geochemistry*, H. D. Holland, K. K. Turekian, Eds. (Elsevier, London, vol. 6, 2003), pp. 1–21.
- R. A. Feely et al., *Global Biogeochem. Cycles* **16**, 1144 (2002).
- S. Chung et al., *Global Biogeochem. Cycles* **17**, 1093 (2003).
- S.-N. Chung et al., *Limnol. Oceanogr.* **49**, 315 (2004).
- C. L. Sabine, R. M. Key, R. A. Feely, D. Greeley, *Global Biogeochem. Cycles* **16**, 1067 (2002).

- L. A. Anderson, J. L. Sarmiento, *Global Biogeochem. Cycles* **8**, 65 (1994).
- S. Kanamori, H. Ikegami, *J. Oceanogr. Soc. Jpn.* **38**, 57 (1982).
- The details of the methods for determining the CaCO₃ dissolution are given in the supporting online materials.
- D. Iglesias-Rodriguez et al., *Eos* **83**, 365 (2002).
- K. Lee, *Limnol. Oceanogr.* **46**, 1287 (2001).
- R. Schiebel, *Global Biogeochem. Cycles* **16**, 10.1029/2001GB001459 (2002).
- N. R. Catubig et al., *Paleoceanography* **13**, 298 (1998).
- W. S. Broecker, T. Takahashi, H. J. Simpson, T.-H. Peng, *Science* **206**, 409 (1979).
- J. A. Kleypas et al., *Science* **284**, 118 (1999).
- T. Takahashi et al., *Deep-Sea Res. Part II* **49**, 1601 (2002).
- S. Reynaud et al., *Global Change Biol.* **9**, 1 (2003).
- F. Marubini, H. Barnett, C. Langdon, M. J. Atkinson, *Mar. Ecol. Prog. Ser.* **220**, 153 (2001).
- A. Sciandra et al., *Mar. Ecol. Prog. Ser.* **261**, 111 (2003).
- K. Simkiss, K. M. Wilbur, *Biom mineralization* (Academic Press, New York, 1989).
- H. A. Lowenstam, S. Weiner, *On Biomineralization* (Oxford Univ. Press, Oxford, 1989).
- A. Mucci, *Am. J. Sci.* **238**, 780 (1983).
- C. Langdon et al., *Global Biogeochem. Cycles* **14**, 639 (2000).
- F. Marubini, B. Thake, *Limnol. Oceanogr.* **44**, 716 (1999).
- M. Spindler, *Neues Jahrb. Geol. Palaontol. Mh.* **9**, 659 (1980).
- H. Pestana, *J. Sediment. Petrol.* **55**, 184 (1985).
- V. J. Fabry, W. G. Deuser, *Deep-Sea Res. Part A* **38**, 713 (1991).
- U. Riebesell et al., *Nature* **407**, 364 (2000).
- I. Zondervan, R. E. Zeebe, B. Rost, U. Riebesell, *Global Biogeochem. Cycles* **15**, 507 (2001).
- H. J. Spero, J. Bijma, D. W. Lea, B. E. Bemis, *Nature* **390**, 497 (1997).
- S. Barker, H. Elderfield, *Science* **297**, 833 (2002).
- N. Gruber et al., in *The Global Carbon Cycle: Integrating Humans, Climate, and The Natural World*. SCOPE 62, C. B. Field, M. R. Raupach, Eds. (Island Press, Washington, DC, 2004), pp. 45–76.
- D. Archer, E. Maier-Reimer, *Nature* **367**, 260 (1994).
- R. A. Armstrong, C. Lee, J. I. Hedges, S. Honjo, S. G. Wakeham, *Deep-Sea Res.* **49**, 219 (2002).
- A. J. Ridgwell, *Geochem. Geophys. Geosyst.* **4**, 1051 (2003).
- F. J. Millero, *Geochim. Cosmochim. Acta* **59**, 661 (1995).
- P. R. Betzer et al., *Science* **224**, 1074 (1984).
- M. Rodier, R. Le Borgne, *Deep-Sea Res. Part II* **44**, 2085 (1997).
- S. Tsunogai, S. Noriki, *Tellus Ser. B Chem. Phys. Meteorol.* **43**, 256 (1991).
- C. S. Wong et al., *Deep-Sea Res.* **46**, 2735 (1999).
- S. Honjo, J. Dymond, R. Collier, S. Manganini, *Deep-Sea Res.* **42**, 831 (1995).
- H. Kawahata, A. Suzuki, H. Ohta, *Deep-Sea Res.* **47**, 2061 (2000).
- S. Noriki, K. Hamahara, K. Harada, *J. Oceanogr.* **55**, 693 (1999).
- We thank all of those that contributed to the global data set compiled for this project, including those responsible for the hydrographic, nutrient, oxygen, carbon, and CFC measurements and the chief scientists. This work was funded by grants from the National Oceanic and Atmospheric Administration, the National Science Foundation, and the Department of Energy. Partial support for K.L. was also provided by the Advanced Environmental Biotechnical Research Center at Pohung University of Science and Technology. This is Pacific Marine Environmental Laboratory contribution number 2633.

Supporting Online Material

www.sciencemag.org/cgi/content/full/305/5682/362/DC1
SOM Text
Fig. S1
Table S1
References

1 March 2004; accepted 8 June 2004